The Orientation Dependence of the Electron Backscattering Coefficient of Gold Single Crystal Films

H. Drescher, E. R. Krefting, L. Reimer, and H. Seidel

Physikalisches Institut der Universität Münster, Elektronenmikroskopische Abteilung

(Z. Naturforsch. **29 a**, 833–837 [1974]; received March 21, 1974)

A theory is developed for calculating the orientation dependence of the backscattering coefficient of single crystal films. Three contributions are calculated separately; firstly the direct backscattering out of the Bloch wave field, secondly the backscattering of electrons scattered out of the wave field into angles smaller than 90° and thirdly the remaining fraction of electrons scattered into very small angles. The electron diffusion is considered by Monte-Carlo calculations. The results are approximated by simple analytical formulas for computation. The theory is compared with experiments on gold single crystal films on a mica substrate. For primary electron energies below 6 keV, a decrease of the orientation anisotropy of backscattering is observed with decreasing energy, whereas Si and Ge single crystals show a further increase. This decrease agrees with numerical calculations using cross sections for low energies.

1. Introduction

The electron backscattering coefficient η of single crystals depends on the angle of incidence of the electron beam on the lattice planes. In scanning electron microscopy one can observe these variations in the form of a channelling pattern. If the direction of the electron beam is rocking on the crystal surface, the signal of backscattered electrons is recorded on a television screen with simultanous scanning. Both experiments and theoretical calculations have been made by several authors to study the intensity of channelling patterns from single crystals in the energy range of some tens of keV [1–7]. A theory of Reimer et al. [2] allows the orientation dependence of the backscattering coefficient for single crystals only to be calculated. This paper improves this theory for the calculation of both bulk material and thin films and combines the Bloch wave field calculation with the consideration of multiple scattering by the Monte-Carlo method. In addition further experiments are presented on Si and Ge single crystals (2 – 10 keV) and on Au single crystal films (2 – 100 keV).

2. Theory of Backscattering of Single Crystal Specimens

The electron wave function inside the crystal is described in terms of Bloch waves:

$$\psi(\boldsymbol{r}) = \sum_j C_0^{(j)} \sum_{\boldsymbol{g}} C_{\boldsymbol{g}}^{(j)} \exp\{2\pi i(\boldsymbol{k}^{(j)} + \boldsymbol{g})\cdot\boldsymbol{r}\} \cdot \exp\{-2\pi q^{(j)} z\}. \quad (1)$$

Reprint requests to Prof. Dr. L. Reimer, Physikalisches Institut der Westf. Wilhelms-Universität, *D-4400 Münster (Westf.)*, Schloßplatz 7.

The eigenvectors $C_{\boldsymbol{g}}^{(j)}$, the wave vectors $\boldsymbol{k}^{(j)}$ and the absorption parameters $q^{(j)}$ can be obtained by standard computer methods for solving the eigenvalue problem (basic equation of the dynamical theory of electron diffraction)

$$[K^2 - (\boldsymbol{k}^{(j)} + \boldsymbol{g})^2 + q^{(j)2} - 2i k_z^{(j)} q^{(j)}] C_{\boldsymbol{g}}^{(j)} + \sum_{\boldsymbol{h}\neq\boldsymbol{g}} U_{\boldsymbol{h}-\boldsymbol{g}} C_{\boldsymbol{h}}^{(j)} + i \sum_{\boldsymbol{h}} U'_{\boldsymbol{h}-\boldsymbol{g}} C_{\boldsymbol{h}}^{(j)} = 0 \quad (2)$$

(K = wave number inside the crystal and $U_{\boldsymbol{g}} + i U'_{\boldsymbol{g}} = (2m/h^2)(1 + E/mc^2)(V_{\boldsymbol{g}} + i V'_{\boldsymbol{g}})$ complex Fourier coefficients of the lattice potential).

To calculate the intensity η of the backscattered electrons three contributions are calculated separately.

1. Direct backscattering out of the Bloch wave field into scattering angles $\vartheta > \pi/2$. The contribution $\mathrm{d}\eta_\mathrm{I}$ from a slice of thickness $\mathrm{d}z$ at a depth z below the surface, with $\mathrm{d}z/V_\mathrm{e}$ unit cells per unit area (V_e = volume of a unit cell), can be expressed in the form

$$\mathrm{d}\eta_\mathrm{I} = \left[\frac{1}{V_\mathrm{e}} \int_{V_\mathrm{e}} \delta(\boldsymbol{r} - \boldsymbol{r}_\mathrm{atom})\, \psi\psi^*\, \mathrm{d}\tau \int_{\pi/2}^{\pi} \frac{\mathrm{d}\sigma_\mathrm{Mott}}{\mathrm{d}\Omega} \cdot \tau(z, z_0, \vartheta)\, 2\pi \sin\vartheta\, \mathrm{d}\vartheta\right] \frac{\mathrm{d}z}{V_\mathrm{e}}. \quad (3)$$

The probability for the interaction of the wave field with the atoms of the unit cell is assumed to be a delta function concentrated at each site of a nucleus. $\mathrm{d}\sigma_\mathrm{Mott}/\mathrm{d}\Omega$ is used for the differential cross section [2, 8, 9]. An electron leaving the wave field at a depth z of a film of total thickness z_0 into a scattering angle $\vartheta > \pi/2$ has the probability $\tau(z, z_0, \vartheta)$ of leaving the surface. $\tau(z, z_0, \vartheta)$ is not the mere

transmission coefficient of an electron beam with an inclination angle $\pi-\vartheta$ through a film of thickness z. In particular if $\pi-\vartheta$ is near 90° electrons can be scattered forwards again and can diffuse by multiple scattering in the whole film thickness z_0.

2. Indirect backscattering out of the Bloch wave field into angles $10°<\vartheta<\pi/2$. The corresponding contribution is

$$\mathrm{d}\eta_{\mathrm{II}}=\left[\frac{1}{V_e}\int_{V_e}\delta(\boldsymbol{r}-\boldsymbol{r}_{\mathrm{atom}})\,\psi\,\psi^*\,\mathrm{d}\tau\int_{10°}^{\pi/2}\frac{\mathrm{d}\sigma_{\mathrm{Mott}}}{\mathrm{d}\Omega}\cdot\eta(z,z_0,\vartheta)\,2\pi\sin\vartheta\,\mathrm{d}\vartheta\right]\frac{\mathrm{d}z}{V_e}\qquad(4)$$

where $\eta(z,z_0,\vartheta)$ is the probability that an electron leaving the wave field at a depth z at an angle $\vartheta<\pi/2$ will be backscattered in the layer z_0-z and also penetrate the upper layer of thickness z. The lower boundary $\vartheta=10°$ of the integral is arbitrary, because this boundary also appears in the next contribution of small angle scattering.

3. Indirect backscattering of electrons out of the wave field into small angles. The total intensity

$$I(z)=\sum_{\boldsymbol{g}}\sum_{i,j}C_0^{(i)}\,C_{\boldsymbol{g}}^{(j)*}\,C_{\boldsymbol{g}}^{(i)}\,C_{\boldsymbol{g}}^{(j)*}\cos\left(2\pi(\boldsymbol{k}^{(i)}-\boldsymbol{k}^{(j)})z\right)\cdot\exp\left\{-2\pi(q^{(i)}+q^{(j)})z\right\}\qquad(5)$$

of the Bloch waves is decreased by $\left|\partial I(z)/\partial z\right|\mathrm{d}z$ in a slice of thickness $\mathrm{d}z$. This decrease includes elastically as well as inelastically scattered electrons. We subtract all electrons considered in (3) and (4) from this value and get the difference

$$f(z)\,\mathrm{d}z=\left|\frac{\partial I(z)}{\partial z}\right|\mathrm{d}z-\left[\int_{10°}^{\pi}\frac{\mathrm{d}\sigma_{\mathrm{Mott}}}{\mathrm{d}\Omega}\,2\pi\sin\vartheta\,\mathrm{d}\vartheta\cdot\frac{1}{V_e}\int_{V_e}\delta(\boldsymbol{r}-\boldsymbol{r}_{\mathrm{atom}})\,\psi\,\psi^*\,\mathrm{d}\tau\right]\frac{\mathrm{d}z}{V_e}.\qquad(6)$$

This consists of electrons scattered elastically into angles $\vartheta<10°$ and those scattered inelastically out of the wave field. Those scattered inelastically are assumed to be concentrated at small scattering angles. All these electrons fall almost normal onto the layer of thickness z_0-z. The special backscattering coefficient $\eta(z,z_0,\vartheta)$ does not show large variations for small ϑ and we therefore use $\eta(z,z_0,\vartheta=0)$. The third contribution can be expressed as

$$\mathrm{d}\eta_{\mathrm{III}}=f(z)\,\eta(z,z_0,\vartheta=0)\,\mathrm{d}z.\qquad(7)$$

As $\mathrm{d}\eta=\mathrm{d}\eta_{\mathrm{I}}+\mathrm{d}\eta_{\mathrm{II}}=\mathrm{d}\eta_{\mathrm{III}}$, the total backscattering intensity is given by

$$\eta=\int_0^{z_0}(\mathrm{d}\eta/\mathrm{d}z)\,\mathrm{d}z=\eta_{\mathrm{I}}+\eta_{\mathrm{II}}+\eta_{\mathrm{III}}.\qquad(8)$$

The values $\eta(z,z_0,\vartheta)$ and $\tau(z,z_0,\vartheta)$ can be obtained from Monte-Carlo calculations [9]. For an easier evaluation of the angular dependent integrals in (3) and (4) we used the following approximations which are in good agreement with the Monte-Carlo calculations (Figs. 1 and 2):

$$\eta(z,z_0,0)=A(z_0)\exp\left\{-B(z_0)z\right\}-C(z_0),\qquad(9\,\mathrm{a})$$

$$\eta(z,z_0,\tfrac{1}{2}\pi)=\eta(0,z_0,\tfrac{1}{2}\pi)\,(1-z/z_0),\qquad(9\,\mathrm{b})$$

$$\eta(z,z_0,\vartheta)=\eta(z,z_0,0)\exp\left\{D(1-\cos\vartheta)\right\}\qquad(9\,\mathrm{c})$$

$$\text{with } D=\ln\left\{\eta(z,z_0,\tfrac{1}{2}\pi)/\eta(z,z_0,0)\right\},$$

$$\tau(z,z_0,\vartheta)=\tau(z,z_0,\pi)+\frac{4}{\pi^2}(\pi-\vartheta)^2\left(\eta(z,z_0,\tfrac{1}{2}\pi)-\tau(z,z_0,\pi)\right).\qquad(9\,\mathrm{d})$$

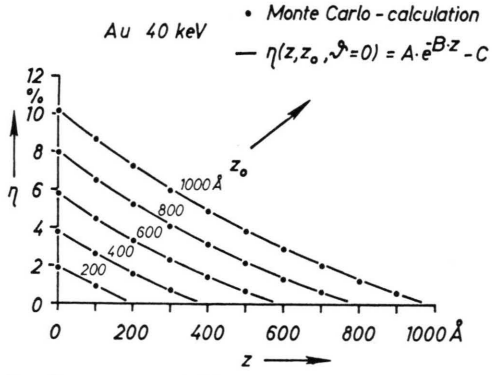

Fig. 1. Comparison of Monte-Carlo calculations with the analytic approximation of $\eta(z,z_0,0)$ by (9 a).

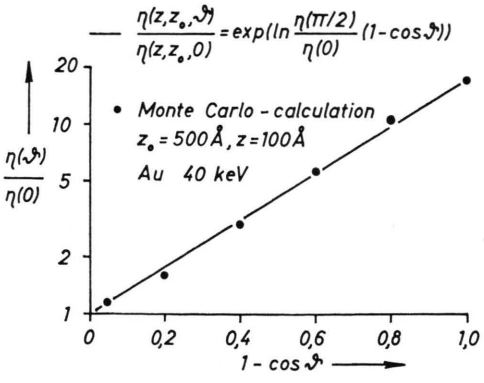

Fig. 2. Comparison of Monte-Carlo calculations with the analytic approximation of $\eta(z,z_0,\vartheta)$ by (9 c).

This theory can equally well be applied to thin specimens as well as to bulk material. No "cut-off

thickness" is required, since for crystal thickness $z_0 \to \infty$ all values in (3), (4) and (7) depending on z_0 converge to the corresponding values for bulk material. The effects of multiple scattering are incorporated in $\eta(z, z_0, \vartheta)$ and $\tau(z, z_0, \vartheta)$ which depend on the film thickness z_0. Thus for $z_0 \to \infty$ the total backscattering intensity tends to a saturation value.

Equations (3), (4) and (7) can be solved more easily if the interference terms between the different Bloch waves are omitted. However, since experiments on the characteristic X-ray production in thin crystals [10] show the importance of these terms, we evaluated (3), (4) and (7) with them included and did not use the independent Bloch wave model.

Since the calculation of a complete rocking curve in the 37-beam case requires too much computer time, the calculations were carried out for the 7-beam case across the $2\bar{2}0$-row of gold, using 40 keV electrons. Figures 3 a, b show two examples of the angular dependence of η near the 111-pole of a gold single crystal film. The angle of incidence is represented by the parameter k_x/g, where k_x is the component of the wave vector of the incident beam parallel to $\boldsymbol{g}$ (excitation of the $2\bar{2}0$-reflex for $k_x/g = 0.5$). One sees that a 100 Å film shows a larger relative variation of the backscattering coefficient than a thicker one. To examine the contributions I – III to the variation of η, the maximum difference $\Delta\eta_{\max} = \eta(k_x/g = 0) - \eta(k_x/g = 1.25)$ is plotted in Fig. 4 as a function of film thickness z_0. The contribution η_{I} is saturated at nearly 100 Å. This is the order of magnitude of the depth of the Bloch wave field. A further increase of anisotropy is caused by the contribution η_{II}. This contribution increases linearly with film thickness up to 1000 Å. The diagram also contains some experimental results. The theoretical curves are obtained from 37-beam calculations because for $\Delta\eta$ only $\eta(k_x/g = 0)$ and $\eta(k_x/g = 1.25)$ are needed.

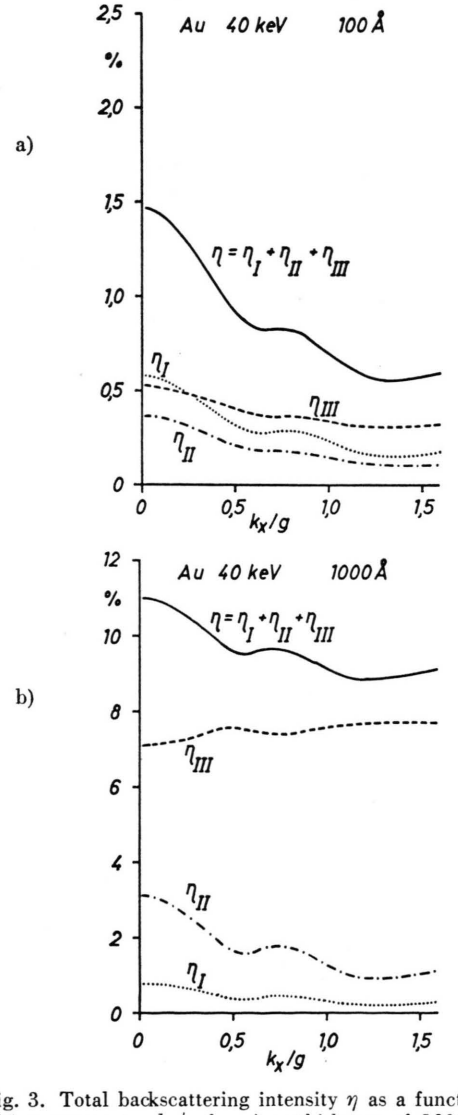

Fig. 3. Total backscattering intensity η as a function of the tilting parameter k_x/g for a) a thickness of 100 Å and b) 1000 Å (full curves) and the three contributions η_{I}, η_{II}, and η_{III}.

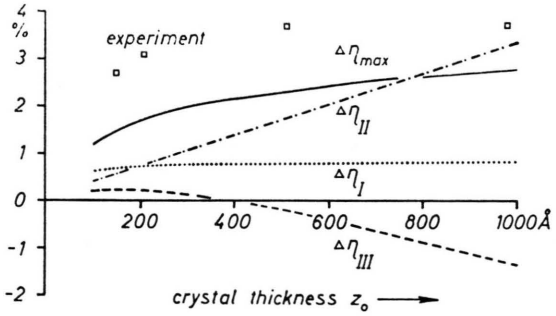

Fig. 4. Maximum variation $\Delta\eta_{\max}$ as a function of single crystal film thickness and experimental values.

3. Experiments

Experiments were carried out on Au single crystal films obtained by epitaxial evaporation onto cleaved mica at 330 °C. The mica sheet has only a small influence on backscattering. Figures 5 a, b show recorded backscattering coefficients (full curve) when tilting the specimen. At 9 and 40 keV the thickest Au film shows the same backscattering

Table 1.

g	V_g (eV)	$V_{g'}$ (eV)
000	—	3.50
220	12.83	1.65
422	6.92	1.29
440	5.72	1.12
642	3.88	0.78
660	3.22	0.59

as bulk material. Calculations were made for the 37-beam case (see Ref. [2]) using the complex potential values $V_g + iV'_g$ of Radi [11] (dotted line). These cannot however explain the size of the variation in η. There is better agreement using the corrected values that are also used in best fit calculations for the convergent beam diffraction technique [12]. The values used here are listed in Table 1. For the discussion of the energy dependence of the variation of η we again used the maximum variation $\Delta\eta_{max}$ between $k_x/g = 0$ and $\cong 1.25$. Figure 6 shows $\Delta\eta_{max}$ for electron energies of 10 – 100 keV. The full curve is obtained from 37-beam calculations. The diagram also contains earlier experiments for Si and Ge single crystals. The smaller values of $\Delta\eta_{max}$ for Au at high energies may be caused by the finite film thickness. The thickness is perhaps not large enough for the higher energies to obtain complete saturation. At low energies (1 – 10 keV) $\Delta\eta_{max}$ shows a maximum for gold films, whereas a further increase with decreasing energy occurs for Si and Ge (Figure 7). One reason for the decrease of $\Delta\eta_{max}$ for Au at low energies is the decrease of the total backscattering coefficient [6], another is the scattering cross section for large angles. Calculations were carried out for three energies (1, 1.5 and

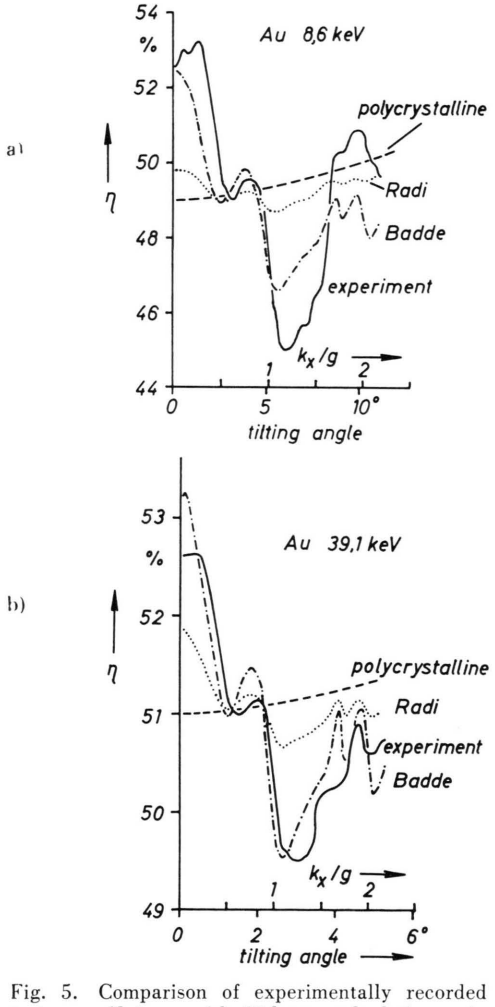

Fig. 5. Comparison of experimentally recorded backscattering coefficients with 37-beam calculation using complex Fourier coefficients of Radi [11] and Badde and Reimer [12] for primary electron energies of a) 8.6 keV and b) 39.1 keV.

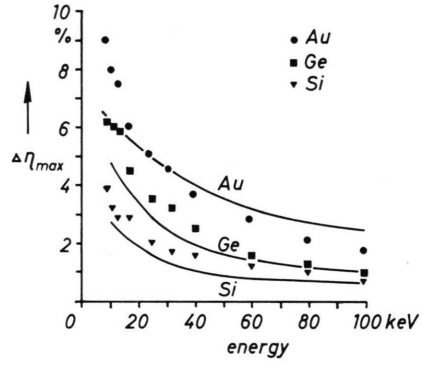

Fig. 6. Experiments and calculations of the maximum variation $\Delta\eta_{max}$ for Si, Ge and Au in the energy range 10 – 100 keV.

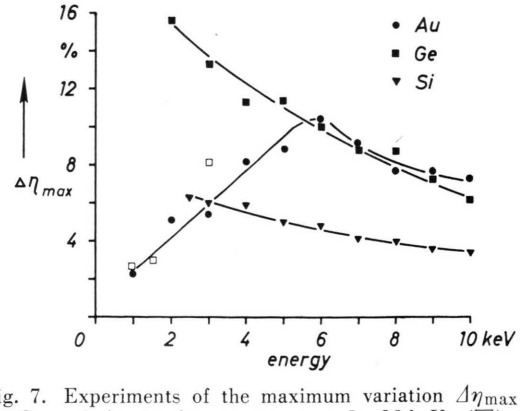

Fig. 7. Experiments of the maximum variation $\Delta\eta_{max}$ for Si, Ge and Au in the energy range 1 – 10 keV. (□) Calculations for Au with scattering cross sections of Holzwarth and Meister [13].

3 keV) using cross sections $d\sigma_{Mott}/d\Omega$ for Hg [13]. Only 7-beam calculations were used because the radius of the Ewald sphere is small at these low energies. The calculations show the right order of magnitude and the right tendency that $\Delta\eta_{max}$ increases with increasing energy below the maximum.

[1] H. Seiler and G. Kuhnle, Z. angew. Physik **29**, 254 [1970].
[2] L. Reimer, H. G. Badde, H. Seidel, and W. Bühring, Z. angew. Physik **31**, 145 [1971].
[3] E. Vicario, M. Pitaval, and G. Fontaine, Acta Cryst. **A 27**, 1 [1971].
[4] J. P. Spencer, C. J. Humphreys, and P. B. Hirsch, Phil. Mag. **26**, 193 [1972].
[5] G. R. Booker, D. C. Joy, J. P. Spencer, and C. J. Humphreys, Proc. 6th Scanning Electron Microscope Symp., IIT Research Institute, p. 251, Chicago 1973.
[6] L. Reimer, Scanning Electron Microscopy: Systems and Applications, p. 120, Inst. of Physics, London-Bristol 1973.
[7] L. Reimer, Beiträge zur elektronenmikroskopischen Direktabbildung von Oberflächen 4/2, 275, Münster 1971.
[8] H. G. Badde, H. Drescher, E. R. Krefting, L. Reimer, H. Seidel, and W. Bühring, Proc. 25th Ann. Meeting of EMAG, p. 79, Inst. of Physics, London-Bristol 1971.
[9] E. R. Krefting and L. Reimer, Quantitative Analysis with Electron Microprobes and Secondary Ion Mass Spectrometry (ed. E. Preuss), p. 114, Kernforschungsanlage Jülich, Germany 1973.
[10] D. Cherns and A. Howie, Z. Naturforsch. **28 a**, 565 [1973].
[11] G. Radi, Acta Cryst. **A 26**, 41 [1970].
[12] H. G. Badde and L. Reimer, Proc. 5th European Congr. on Electron Microscopy, p. 440, Inst. of Physics, London-Bristol 1972.
[13] G. Holzwarth and H. J. Meister, Tables of Asymmetry, Cross Section and Related Functions for Mott Scattering of Electrons by Screened Gold and Mercury Nuclei, München 1964.